THE JOURNAL OF PHYSICAL CHEMISTRY C
A JOURNAL OF THE AMERICAN CHEMICAL SOCIETY

pubs.acs.org/JPCC

Article

Exciton Effects in Low-Barrier GaN/AlGaN Quantum Wells

Arianna Cretì,[‖] David M. Tobaldi,[‖] Mauro Lomascolo,[*] Iolena Tarantini, Marco Esposito, Adriana Passaseo, and Vittorianna Tasco

Cite This: *J. Phys. Chem. C* 2022, 126, 14727−14734

Read Online

ACCESS | Metrics & More | Article Recommendations | Supporting Information

ABSTRACT: Solid-state light sources irradiating in the ultraviolet (UV) spectral region are key components in today's technologies for several applications. Ultrathin GaN layers in AlGaN barriers represent a promising active medium for UV-emitting photonic devices, but a full understanding of their complex excitonic features deserves further investigation. In this work, GaN layers, grown in AlGaN barriers with different heights by metal organic chemical vapor deposition, were studied with the aim to correlate excitonic effects with structural features. It is shown that the UV emission from such structures involves free and bound excitons, as well as free carriers, while the free exciton binding energy is directly and experimentally derived.

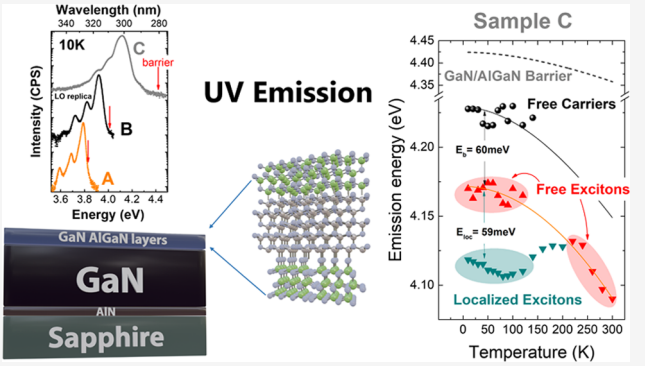

1. INTRODUCTION

The interest in developing novel solid-state light sources covering the ultraviolet spectral region is founded on critical technological applications,[1] such as UV curing; environmental sensing; air, water, and food disinfection; or solar-blind communication.[2] UV light-emitting diodes (LEDs), as an alternative solution to replace unsustainable Hg gas-filled lamps,[3] can even be exploited to inactive pathogens like human coronaviruses.[4]

AlGaN-based semiconductor heterostructures are among the most promising candidates to cover such an optoelectronic window of interest because of their large and direct band gap. However, as depicted in recent reviews,[1,5] there are still several obstacles to be tackled for this technology, hindering the achievement of high external quantum efficiency in AlGaN-based UV LEDs. Generally speaking, structural and, consequently, optical properties of nitride Quantum Wells (QWs) strongly depend on the strain within the epitaxial multilayer as a result of the mismatch in the (basal) unit cell parameters between different nitrides.[6] As an alternative, in the last few years, attention has been focused on gallium nitride layers with extremely reduced dimensionality, that is, ultrathin or quasi-2D GaN QWs, that can exhibit high quantum confinement, enhanced carrier localization, and a blue shift of their bulk optical emission when inserted in AlGaN matrix. These active regions have recently been demonstrated to be beneficial for efficient UV emission in LEDs[7,8] and laser devices.[9] Interesting features of excitonic properties have been theoretically anticipated and experimentally observed in these systems, such as high exciton binding energy,[10,11] high radiative recombination rate,[9,10] and large energy splitting between dark and bright excitons.[10,12] Additionally, exciton localization has also been widely reported in the literature, typically related to interface roughness,[9,11,13] suggesting that a detailed study on the relationship between structural properties and excitonic effects deserves further investigation.

In most cases, ultrathin GaN layers are included within AlN barriers, a design that can push the emission to the very deep UV limits. However, low-strain conditions, associated with limited Al mole fraction in the barrier, can limit the influence of misfit dislocations in the heterostructure and can, in principle, allow for clearer observation of excitonic effects and properties, such as binding energy, localization, and temperature behavior. For this reason, in the present article, we study the structural and optical properties of thin layers of gallium nitride embedded between AlGaN barriers with an Al concentration lower than 50%.

The heterostructures were grown using metal organic chemical vapor deposition (MOCVD)[7,8] and characterized using high-resolution X-ray diffraction (HR-XRD) and photoluminescence (PL) spectroscopy as a function of excitation power and sample temperature. Results evidenced the critical role played by the Al content modulation in the barrier with respect to both the structural properties, referred to as strain field and threading dislocation density, and the excitonic

Received: June 14, 2022
Revised: August 11, 2022
Published: August 23, 2022

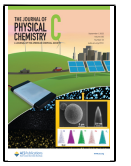

emission from the thin GaN QW, in relationship to its efficiency and the exciton localization behavior and energy.

2. METHODS

2.1. Growth of GaN/AlGaN Short-Period Layers. All epitaxial films used in this study were directly grown on (00.1) *c*-plane Al_2O_3 substrates in a horizontal low-pressure MOCVD system (AIXTRON AIX 200-RF), with NH_3, trimethylgallium (TMGa), and trimethylaluminum (TMAl) as nitrogen, gallium, and aluminum precursors, respectively. H_2 was used as a carrier gas. A 100 nm thick AlN nucleation layer was directly grown on the Al_2O_3 substrate at 1150 °C,[14] followed by 1 μm of high-quality GaN buffer layer with a threading dislocation density of around 3×10^8 cm^{-2}. Then, 20 repetitions of AlGaN/GaN multistacks were grown at the same temperature. The single stack nominally consists of a thin gallium nitride layer ($\leq$1 nm) embedded between AlGaN barriers with different Al compositions. In particular, the Al content was designed to be 15% (sample A), 25% (B), and 40% (C), as we aimed to analyze the early stage of detrimental effects related to AlGaN/GaN multistacking.[15] A schematic of the sample structure is shown in Figure 1a. The conduction

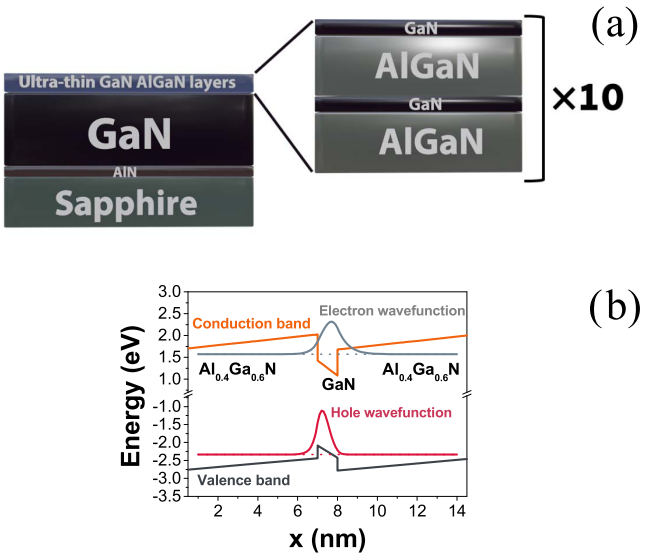

Figure 1. (a) Schematics of the realized samples. (b) Energy diagram profile calculated through nextnano software for conduction and valence bands, electrons' and holes' main eigenvalues, and occupation probability functions (electron and hole wavefunction).

and valence band profiles, along with electron and hole eigenstates, have been calculated in the first approximation using nextnano software[16] and are shown in Figure 1b for the highest Al content sample. While the model does not take into account the strain within the GaN QW, it provides a simplified picture of band profiling expected in this kind of sample.

2.2. Characterization. The structural properties of the GaN/AlGaN QWs were examined with HR-XRD, using a Malvern PANalytical PW 3050/65 X'Pert Pro MRD diffractometer (U.K.) with Cu Kα radiation. To obtain information about structural features of prepared heterostructures, ω–2θ patterns and rocking curves (RCs) were recorded in double-axis configuration, in parallel beam mode, using a parabolic mirror and a four-bounce Ge (220) monochromator; the detector was kept at an open detector configuration. ω–2θ scan simulations were assessed with the X'Pert Epitaxy software package. Thicknesses of the AlGaN/GaN multistacks were taken from XRR fittings, while the Al content in the AlGaN barriers was obtained from the HR-XRD reciprocal space map (RSM) analyses (see below), thus working in an iterative fashion. To minimize effects due to wafer curvature, the beam height was restricted for symmetric RC, whereas for skew-symmetric ω-scans, the beam width was restricted, as suggested by Moram and Vickers.[17] Microstructural features were investigated by collecting RSM around symmetrical (00.2) and asymmetrical ($\overline{1}1.4$) reflections. Furthermore, the crystallographic tilt between the GaN buffer layer and the multistack [00.1] axes from the surface normal direction was assessed by recording ω–φ maps of GaN (00.2) and the GaN/AlGaN pair (00.2) reflections in the azimuthal scanning range of $\varphi = 0$–360°, with a step size of 2.5 °φ. X-ray reflectivity (XRR) analysis was also performed to obtain information about the thickness of the layers. Data were recorded in parallel beam geometry, with an incidence angle from 0 to 8° 2θ. Collected data were modeled with the X'Pert Reflectivity software suite. The model for the fit consisted of 20 repetitions of AlGaN/GaN multistacks over GaN buffer and AlN nucleation layers, as described in Section 2.1. In the XRR fitting, thickness and interface roughness of the AlGaN/GaN multistacks were left as free parameters. The composition of the AlGaN barrier was constrained to that obtained using HR-XRD analyses. The thickness of the GaN buffer and the AlN nucleation layer was constrained to their nominal values.

PL measurements were assessed to investigate the radiative recombination processes and to elucidate the occurrence of extreme quantum confinement in QWs. Spectra were recorded at different temperatures, from 10 K to room temperature, placing the samples on a cold finger of a closed cycle helium cryostat. The excitation beam was delivered by a He-Ag laser (Photon Systems Inc.), operating at 224.3 nm (5.5 eV), a repetition rate of 15 Hz, and a pulse duration of 100 μs. The beam was focused on the sample surface to a spot size of about 10 μm. The PL signal was dispersed through a 0.32 m Triax monochromator (Horiba Ltd) and recorded by a cooled Si-CCD camera (Andor Ltd). The laser excitation power varied among 3 orders of magnitude, from 0.5 to 50 mW (measured on the sample). The photogenerated carrier density at the maximum excitation intensity (I_0 = 50 mW) was estimated to be about $n_0 \sim 2 \times 10^{19}$ cm^{-3} ($\sim 10^{12}$ cm^{-2}), assuming a bulk AlGaN (x = 0.25) absorption coefficient at 224 nm of about 2.3×10^5 cm^{-1}.[18]

3. RESULTS AND DISCUSSION

3.1. Structural and Morphological Analyses. *3.1.1. HR-XRD Analysis.* HR-XRD ω–2θ patterns, together with the simulations of collected data, are displayed in Figure 2a. The GaN (00.2) reflection belonging to the buffer layer (positioned here at zero arcsec) and that belonging to the AlN nucleation layer (at around 2800 arcsec) are clearly visible. Clear Pendellösung fringes can also be detected at the lower-angle side of the AlN reflection. Furthermore, the interference of scattered X-rays forming the multistack resulted in the satellite peaks S_0 and S_{-1}, as shown in Figure 2a. The absence of additional positive-order satellite peaks is due to the overlap with the signal from the buffer and nucleation layers in both measurements and simulations, as shown in Figure S1.

The increase of Al content in the barrier leads to an angular shift of the S_0 satellite peak and an increase of the related full

https://doi.org/10.1021/acs.jpcc.2c04118
J. Phys. Chem. C 2022, 126, 14727–14734

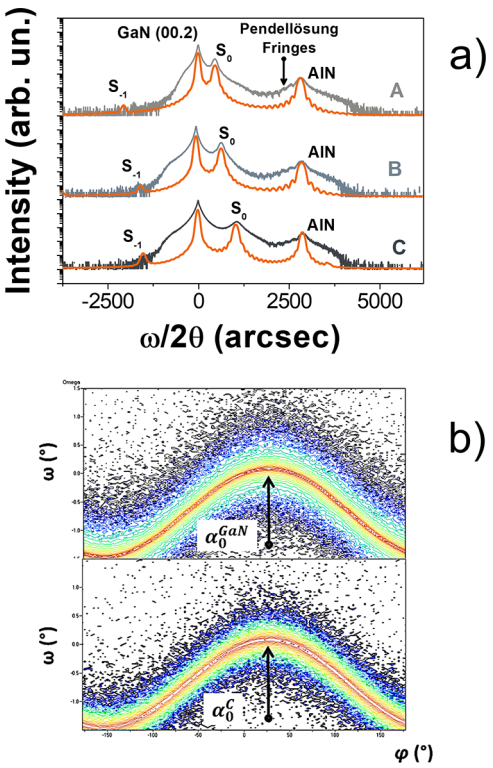

Figure 2. (a) Collected and simulated (orange line) HR-XRD (00.2) $\omega-2\theta$ scans of prepared specimens. Nominal thicknesses of the layers were used for assessing the simulations. (b) $\omega-\varphi$ maps of GaN (00.2) (top) and GaN/AlGaN layer (00.2) (bottom) reflections, sample C.

width at half-maximum (FWHM, from 113 arcsec in A to 233 arcsec in B), suggesting a critical role of this parameter with respect to reduction in the defect density.

The crystallographic tilt of the GaN buffer layer and the multistack [00.1] from the surface normal direction was also estimated by recording $\omega-\varphi$ maps of GaN (00.2) and S_0 (00.2) reflections (Figure 2b). Tilt angles, as found from the procedure described in detail in the Supporting Section, are very small for all of the samples, in the order of 0.01°, as listed in Table S1, suggesting overall vertical coherence in the grown multistacks.

Afterward, RSMs along with different reflections were collected. The Al content in the AlGaN barriers was calculated from the RSM (00.2) (Figure 3a) using Vegard's law and the method proposed by Angerer et al.,[19] and the results are listed in Table 1. The comparison of the RSM maps from the symmetrical reflection (00.2) confirms a coherent growth of the multistack in the three cases (Figures 3a and S2). On the other hand, assuming the multilayer to consist of randomly misoriented mosaic blocks, their lateral correlation length, along with the spread of the mosaic blocks, was estimated from asymmetric RSM (Figures 3b, and S2). Data obtained *via* the X'Pert Epitaxy software suite are listed in Table 1 and give an insight into the mosaicity of the heterostructures. In particular, they highlight that lowering the Al content in the barrier layers, even though in such a limited range, leads to a significant increase in the lateral correlation length (L_C), together with a decrease in the mosaic spread (M_S).[17]

Symmetrical and asymmetrical reflection RSMs (Figures 3a,b and S3a,b), along with the model by Kaganer,[20] were used to extract the structural parameters of the GaN QW and the AlGaN barrier, in-plane and out-of-plane strain ($\varepsilon_{a\|}$ and $\varepsilon_{\perp}$, respectively) and lattice mismatch (f), that are listed in Table 1. The followed procedure is reported in Supporting materials Section S1.

Further analysis was performed by collecting the RC of AlGaN (12.3) asymmetric reflection (Figure S4). Its incidence angle ω is around 0.7°; therefore, the contribution from the substrate is minimized, and a better resolution is obtained directly for the GaN/AlGaN multilayer signal.[21] Still employing the fitting model described in ref 20, as shown in Figure S4, we have accurately estimated the dislocation density within the GaN/AlGaN stack; *cf* Table 1, 8th column. From the data, it is clear that the variations in Al content, albeit within the limited investigated range, have a dramatic impact on the strain field affecting the confined layer. For low Al content in the AlGaN layer (samples A and B), the in- and out-of-plane strain components and misfit parameters lead to a significantly lower value of total dislocation density, which reduces itself by a factor of 6, as compared with sample C.

3.1.2. XRR Analysis. Specular XRR is insensitive to the deformation in the unit cell parameters. Thus, Kiessig fringes are solely caused by the interference of the waves that are reflected at the surface of the layers.[23] This implies that the period of the oscillation (i.e., the Kiessig fringes) is ruled by the thicknesses associated with the GaN QW and the AlGaN barrier. XRR patterns of the three heterostructures are displayed in Figure 4. The thickness of the GaN QW and that of the AlGaN barrier layers, as extracted from the fitting, are reported in Table 2, in line with nominal values.

3.2. Optical Characterization. Representative PL spectra recorded at 10 K for each sample are reported in Figure 5a. The red arrows indicate the $Al_xGa_{1-x}N$ energy gap as predicted for bulk layers by Vurgaftman et al.[24] The values of the Al content were those obtained by XRD analyses. As expected, the emission signal of samples A and B with lower confinement is almost resonant to the corresponding barrier energy value. On the other hand, sample C shows a broad PL spectrum, at high energy, ~300 meV below the energy barrier, due to the deeper confinement, in good correlation with band profile schematic calculations (see Figures 1 and S5).

Common features are highlighted from the PL spectra. An intense band, occurring at ~3.80 eV (sample A), ~3.92 eV (sample B), and ~4.11 eV (sample C), dominates the emission at high energy, while phonon replicas are clearly observed at the low-energy side of the spectra (dotted lines in Figure 5b) attributed to bulk GaN longitudinal optical (LO) phonon, given the interspacing of 92 meV.[25]

A detailed multipeak Gaussian analysis of PL spectra reveals a quite rich structure for all of the samples (see Figure 5b, top panel, for sample B and Figure S6a,c for samples A and C). In particular, the highest energy band consists of four components (x_i transitions, continuous lines in Figure 5b). Given their energy position, they can be related to the AlGaN barrier and/or to the GaN QW emission, where, in turn, different exciton complexes (free excitons, localized excitons, bound excitons, *etc.*) and free-carrier recombination are typically observed.[26,27] Therefore, further investigation is needed for a clear attribution. In Table S2 are reported the energy values of x_i transitions for all of the samples.

PL experiments at low temperatures have been performed as a function of excitation intensity, from 0.5 to 50 mW. The spectra related to sample B are shown in Figure 5b. Gaussian analysis reveals that the first two transitions in the high-energy region (x_1 and x_2) only appear for excitation intensity >0.1 I_0

https://doi.org/10.1021/acs.jpcc.2c04118
J. Phys. Chem. C 2022, 126, 14727−14734

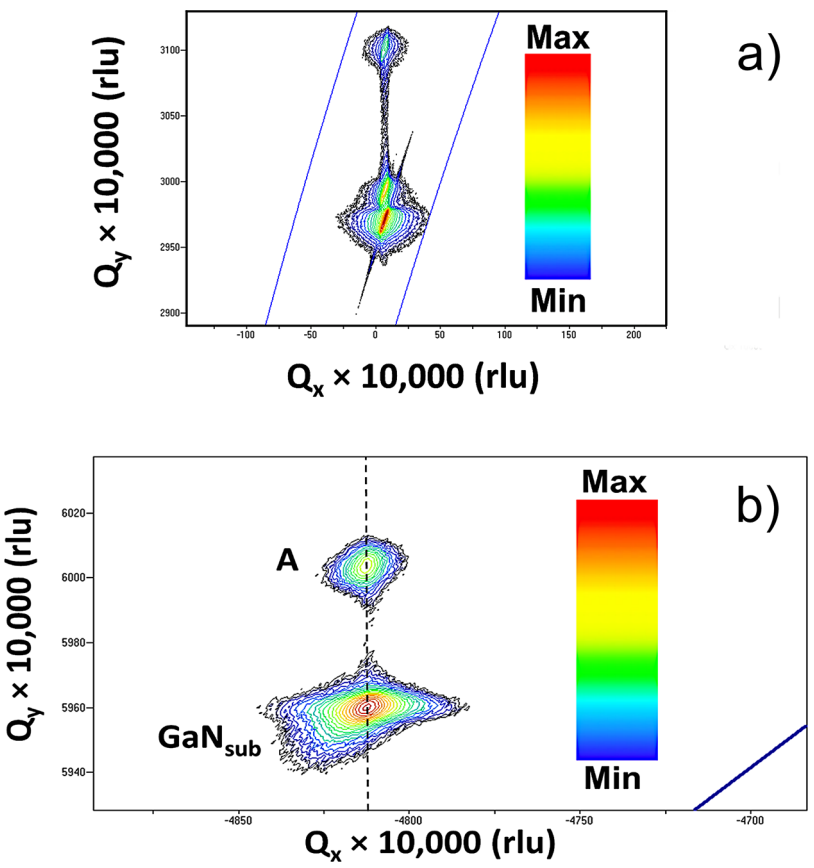

Figure 3. (a) RSM along the (00.2) reflection, A. (b) RSM along the $(\overline{1}1.4)$ reflection, A. The vertical dashed line represents the position at which the strained GaN/AlGaN epilayers are supposed to be.

Table 1. Al Content (x) in the AlGaN Layer from Vegard and Angerer et al.[19]

sample	*x*, Vegard (relaxed)	*x*, Angerer (strained)	L_c (nm)	M_s (arcsec)	$\varepsilon_{a\parallel}$ GaN(AlGaN) (%)	$\varepsilon_{\perp}$ GaN(AlGaN) (%)	|*f*| (%)	$\rho_{SL} \times 10^9$ cm^{-2}
C	0.37	0.35	26	410	−0.20 (0.69)	0.10 (−0.40)	1.01	7.4
B	0.24	0.22	62	158	−0.11 (0.46)	0.02 (−0.31)	0.46	3.9
A	0.16	0.15	84	47	−0.09 (0.28)	0.04 (−0.17)	0.42	1.3

Bulk GaN and AlN unit cell parameters were taken from Wallis et al.[22] Dislocation density in the AlGaN barrier and structural parameters of GaN/AlGaN layers as obtained from HR-XRD RSM analysis.

(black and red vertical dashed lines in the figure). On the other hand, at very low excitation intensity (0.01 I_0), only the band corresponding to *the* x_3 Gaussian component remains visible. Similar behavior is observed in all of the samples (Figure S6a,c for samples A and C).

Emission experiments have been also performed as a function of temperature in the range of 10−300 K. To interpret the origin of the weak emission bands observed in the high-energy shoulder of PL emission (x_1 and x_2), spectra were recorded with the maximum available excitation intensity (I_0 = 50 mW). A representative set of PL spectra at different temperatures is reported in Figure 6a, again for sample B (x = 0.23). Spectra for the other samples are shown in Figure S7. As a general trend, in all of the investigated samples, QW complex emission features (*e.g.*, for sample B, the one at about 3.9 eV, Figure 6a) are quenched by about 4 orders of magnitude as the temperature is increased, and only the main band x_3 is observed up to room temperature.

In Figure 6b, the Gaussian energy peaks for each investigated sample are reported as a function of temperature. The continuous lines represent a fit carried out on the high-temperature experimental data for the main bands using the Varshni empirical formula, extrapolated to 10 K.[29] Finally, the dashed lines represent the AlGaN barrier energy gap (as obtained from Vurgaftman et al.)[24] for the different Al concentrations.

In all of the samples, the most intense peak x_3 shows an *S*-shaped temperature trend, typically associated with exciton localization effects in similar material systems.[9,30,31] Additionally, at high temperatures, it follows Varshni's law related to the free exciton recombination at the value expected for these structures. We highlight that, for each sample, the emission energy of the x_3 band well matches the values provided by the first-principles calculations based on density functional theory, as reported by Wang et al.[32] for similar heterostructures (Figure S8), namely, for thin GaN QWs of few monolayers (one to two monolayers) and AlGaN barrier (with varying Al content). The former analysis leads to attributing this emission feature to the excitonic emission, which is also expected to have a large oscillator strength.[33] The exciton localization energy values, estimated as the difference between the exciton PL resonance at low temperatures, in which the exciton

https://doi.org/10.1021/acs.jpcc.2c04118
J. Phys. Chem. C 2022, 126, 14727−14734

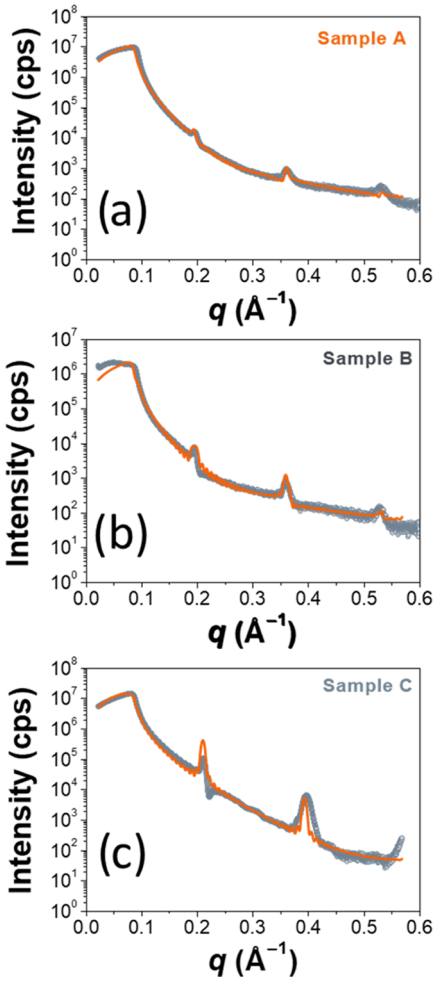

Figure 4. XRR patterns of samples (a) A, (b) B, and (c) C. Light blue circles represent the observed data, and the continuous orange line the fittings.

Table 2. Thickness of the GaN QW and AlGaN Barrier as Extracted from the Fitting of XRR Patterns

	thickness (nm)		
Layer	A	B	C
GaN QW	0.6 ± 0.2	0.5 ± 0.1	0.6 ± 0.1
AlGaN barrier	6.6 ± 1.4	6.7 ± 0.1	5.9 ± 0.1

localization is effective, and the value extrapolated at 10 K by Varshni's law related to the free exciton emission (experimentally observed at a higher temperature), are of the same order of magnitude as those observed in similar structures.[9,11,13]

The exciton localization is expected as a consequence of well-width fluctuations and/or related to the well/barrier interface quality, rather than barrier composition fluctuations.[11] Moreover, in the investigated samples, the localization energy clearly increases with Al content in the barrier (31 meV, 37 meV, and 59 meV for A, B, and C, respectively). This result is likely related to a combination of two distinct effects, both related to increased Al content in the barrier, which in turn induces different potential fluctuation relative amplitudes: (i) different interface compositional fluctuations and disorder and (ii) an increased exciton quantum confinement. The trend of the FWHM values of x_3 as a function of the temperature is shown in Figure 6d. The broadening increases with the Al content in the barrier, in line with the increased strain observed by XRD analysis. Additionally, the effect of exciton localization is clear for samples B and C. In correspondence with the switching temperature at which the localized exciton becomes free (about 150 and 200 K for samples B and C, respectively, see Figure 5b), the broadening suddenly decreases, as expected for exciton delocalization processes.[9] For sample A, where confinement is weak, the effect is less pronounced.

In Figure 6c, the internal quantum efficiency (IQE), defined as the integrated Gaussian area of the main transitions (x_3) normalized to its value at 10 K, is reported as a function of temperature for each sample. In particular, the IQE values at 300 K (see Table 3) show that sample A is the most efficient. Indeed, the Al content, modulating the dislocation and defect density, as previously discussed, significantly reduces the emission efficiency in sample C.

Finally, the dotted lines in Figure 6c represent Arrhenius fit using two activation energies (see Section S2, Optical Properties). Both E_{a1} and E_{a2} do not match the exciton localization energies. Therefore, as they cannot be related to exciton delocalization and consequent dissociation mechanism, they should arise from nonradiative recombination processes. In detail, E_{a1} is consistent with the values reported in the literature for similar structures[8] associated to point defects, which are very effective in IQE quenching mechanisms.[30] On the other hand, the process associated with E_{a2} activation energy is not clear, which is significantly smaller than those reported in ref 8, 11.

In all of the samples, the x_4 band shows a behavior similar to the x_3 band (see Figure 6b). In particular, in the less confined samples, A and B, it appears very close in energy to x_3, thus suggesting the same attribution. It can therefore be correlated with excitonic emission, with localization energy almost similar to that of the x_3 band. In sample C, in which the larger barrier induces greater confinement, the energy separation between x_3 and x_4 is more prominent (almost 35 meV at 10 K). The temperature trend of the x_4 band, which disappears at almost 100 K, maintaining an almost constant value rather than an *S*-shape and/or a Varshni-like trend, does not allow for easy identification/attribution. However, its existence is a further indication of the increased complexity of energy level structuring in sample C, due to the increased Al content in terms of increased confinement and/or worsening structural quality.

The attribution of the transitions at high energy, namely, x_1 and x_2, deserves further discussion. In all of the samples, the x_2 PL band is observed only at low temperature and at high excitation intensity, and its integrated area is 2 orders of magnitude lower than that of x_3. Additionally, the temperature trend of the x_2 Gaussian peak is well described by the Varshni empirical formula, extrapolated to 10 K, as previously discussed. In particular, it fits the trend of the free exciton recombination, previously identified by the x_3 band (Figure 6b). Therefore, we can conclude that the x_2 band originates from the small amount of the free exciton population in thermal equilibrium with that of the localized exciton at low temperatures. In fact, for the lowest excitation intensities (at 10 K), the x_2 band is not visible (see Figures 5b and S5a) due to the dominance of the localized exciton contribution (x_3 emission band).

The x_1 Gaussian components, observed only at low temperature, follow, in the shallower samples A and B, the

https://doi.org/10.1021/acs.jpcc.2c04118
J. Phys. Chem. C 2022, 126, 14727−14734

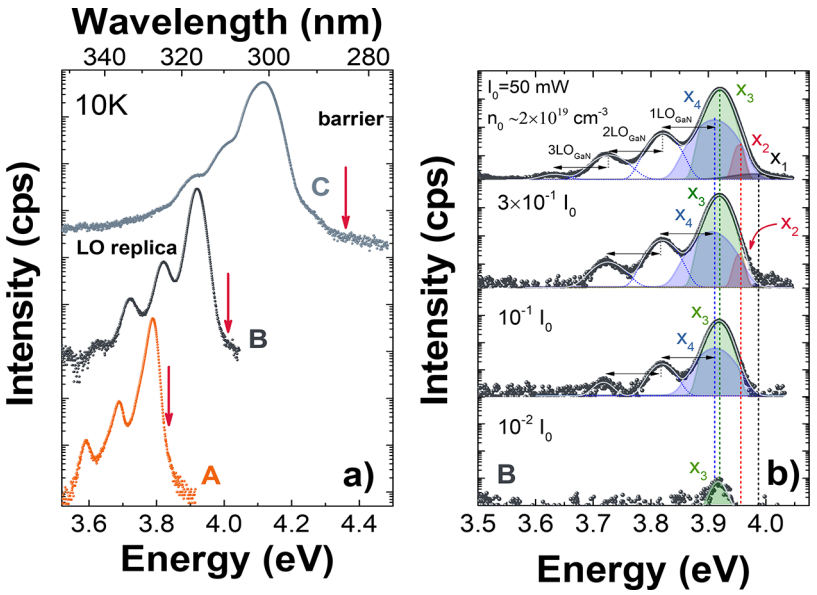

Figure 5. (a) PL spectra recorded at 10 K for the GaN/$Al_xGa_{1-x}N$ heterostructure; from bottom to top, samples A (orange), B (gray), and C (light gray). The red arrows point to the $Al_xGa_{1-x}N$ energy gap as predicted by Vurgaftman et al.[24] (b) Representative multi-Gaussian analysis performed on sample B at different excitation intensities. Blue dotted lines represent the phonon replica components. Horizontal arrows show LO phonon energy (~92 meV); vertical colored dashed lines indicate the energy position of the principal components at higher energy (namely, x_1, x_2, x_3, x_4). The maximum power I_0 is 50 mW corresponding to a photogenerated carrier density of about n_0 ~2 × 10^{19} cm^{-3} (~10^{12} cm^{-2}). PL spectra have been vertically stacked with offset for clarity.

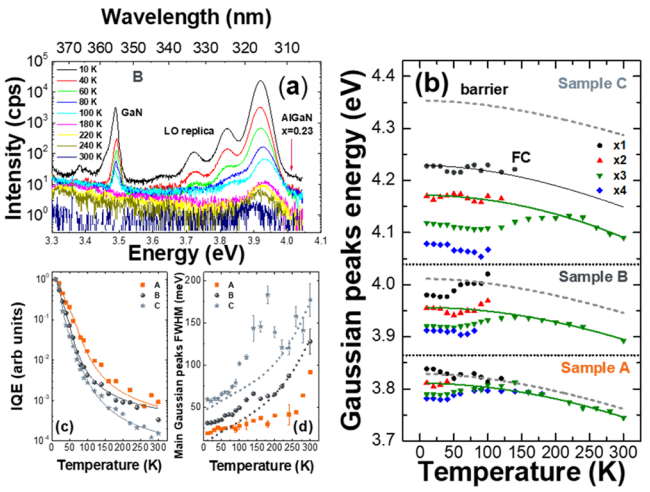

Figure 6. (a) Selected PL spectra recorded as a function of temperature in the range of 10−300 K for sample B. The red arrow indicates the $Al_xGa_{1-x}N$ energy gap predicted by Vurgaftman et al.[24] (b) Gaussian PL peak energy (x_i, symbols) as a function of temperature for each sample. Continuous lines represent Varshni empirical formula fits. AlGaN barrier energy, as predicted by Vurgaftman et al.,[24] is also reported by dashed curves. (c) IQE defined as the integrated Gaussian area of the main peak divided by its value at 10 K as a function of temperature. The dotted lines represent Arrhenius fit using two activation energies. (d) FWHM for the main Gaussian band (x_3) as a function of temperature. Dashed lines represent the Bose−Einstein model fit of the high-temperature experimental data.[28]

AlGaN barrier energy trend predicted by Vurgaftman et al.[24] (dashed curves in the figure). On the other hand, in sample C, with the highest barrier energy, the x_1 band (black circles) is located well below the predicted $Al_{0.40}Ga_{0.60}N$ barrier (dashed line) and about 60 meV above the x_2 band (Figure 6b upper panel, red triangles). Additionally, as long as the x_1 band is visible (up to 150 K), it follows a Varshni behavior (dotted line through the data). This finding strongly suggests that the observed x_1 transition can be related to free-carrier recombination originating from the e−h confined states inside the QWs. In this context, it deserves to be stressed that at the maximum excitation intensity (I_0 = 50 mW) used in this experiment, the corresponding photogenerated carrier excitation density is n_0 ~2 × $10^{19}$$cm^{-3}$ (~10^{12} cm^{-2}), very close to the Mott critical density for exciton dissociation predicted for these structures.[10] Additionally, the observed energy separation between this band and that related to free exciton x_2 (60 meV) is consistent with the binding energy values of the free exciton predicted/observed in ultrathin GaN/(Al,Ga) N-based heterostructures.[11,34] We highlight that such a large exciton binding energy confirms the possibility to obtain in these structures a stable excitonic emission up to room temperature (binding energy value larger than k_BT value at RT).

The high exciton binding energy value is a fundamental characteristic of these systems, and it is typically obtained by comparing the predicted theoretical value for the electronic gap with the experimental optical gap after having established that the emission spectrum is related to free exciton and nonlocalized exciton, rather than free-carrier emission.[35−37] Conversely, in our experiments, the excitation regime induces a

Table 3. Exciton Localization Energies as Reported in Figure 6b, Activation Energies E_{a1} and E_{a2} as obtained by Arrhenius Plot Analysis and Reported in Figure 6c, and Efficiency Parameter IQE at 300 K

sample	exciton localization energy meV	E_{a1} meV	E_{a2} meV	IQE (300 K) × 10^{-4}
A	31	7.6 ± 0.8	38 ± 3	8
B	37	5.2 ± 0.8	27 ± 1	5
C	59	10.7 ± 0.3	42 ± 2	1

https://doi.org/10.1021/acs.jpcc.2c04118
J. Phys. Chem. C 2022, 126, 14727−14734

more complex situation, in which the coexistence of several emitter contributions (excitation at highest intensity) can be observed in the emission spectrum. It was therefore possible to experimentally identify them (free and/or localized exciton, free carriers) by their unique characteristics, and, at least for the most confined sample, the fundamental optical emission properties have been directly measured, namely, the optical gap (from free exciton emission contribution) and the exciton binding energy.

4. CONCLUSIONS

In conclusion, we have thoroughly analyzed heterostructures with GaN QWs within the AlGaN barrier as potential emitters in the deep UV spectral range. The structural properties are found to be closely related to compositional variation, even though coherent growth is observed in the investigated low-strain regime. A full investigation was performed on the excitonic effects arising in such systems. Emission quantum efficiency decreases as the Al content increases, as an effect of the increased strain and reduced crystalline quality of the multilayer, inducing nonradiative recombination processes related to capturing centers. The Al content in the barrier induces different interface compositional fluctuations and disorder, accompanied by different exciton quantum confinements, thus leading to variation in the exciton localization energy. In addition, we have observed and clearly identified free carriers and free exciton emission contribution in the PL signal. We highlight that, at room temperature, the PL signal is only related to the contribution of free exciton radiative recombination. The direct evaluation of exciton binding energy through spectroscopy experiments provides a large exciton binding energy (exceeding the k_BT at room temperature), thus ensuring exciton stability up to room temperature.

■ ASSOCIATED CONTENT

Supporting Information

The Supporting Information is available free of charge at https://pubs.acs.org/doi/10.1021/acs.jpcc.2c04118.

Band profile calculations of the three heterostructures, as obtained via the nextnano software suite; details concerning HR-XRD structural analysis; multi-Gaussian analysis of low-temperature PL spectra; PL spectra recorded as a function of excitation intensity and sample temperature; transition emission energy (optical gap) for ultrathin GaN QW in AlGaN barriers; and details on Arrhenius analysis and PL broadening (FWHM) (PDF)

■ AUTHOR INFORMATION

Corresponding Author

Mauro Lomascolo − *CNR-IMM, Institute for Microelectronic and Microsystems, 73100 Lecce, Italy;* orcid.org/0000-0002-2851-8552; Email: mauro.lomascolo@cnr.it

Authors

Arianna Cretì − *CNR-IMM, Institute for Microelectronic and Microsystems, 73100 Lecce, Italy;* orcid.org/0000-0003-0389-660X

David M. Tobaldi − *CNR-Nanotec, Nanotechnology Institute, 73100 Lecce, Italy;* orcid.org/0000-0002-0112-8570

Iolena Tarantini − *Mathematics and Physics Department, University of Salento, 73100 Lecce, Italy*

Marco Esposito − *CNR-Nanotec, Nanotechnology Institute, 73100 Lecce, Italy;* orcid.org/0000-0001-8170-6694

Adriana Passaseo − *CNR-Nanotec, Nanotechnology Institute, 73100 Lecce, Italy*

Vittorianna Tasco − *CNR-Nanotec, Nanotechnology Institute, 73100 Lecce, Italy;* orcid.org/0000-0002-3392-0976

Complete contact information is available at: https://pubs.acs.org/10.1021/acs.jpcc.2c04118

Author Contributions

‖A.C. and D.M.T. contributed equally to this work. The manuscript was written through the contributions of all authors. All authors have given approval to the final version of the manuscript.

Notes

The authors declare no competing financial interest.

■ ACKNOWLEDGMENTS

The authors are grateful to the project EleGaNTe − PON ARS01_01007 (CUP: B91G18000200005) for funding this research work. The regional project "Innonetwork nmSensors TransfoClean" (CUP: B37H17005010007) funded by InnovaPuglia is also acknowledged. ML and AC acknowledge Giovanni Montagna for his valuable technical help during the optical experiments.

■ REFERENCES

(1) Kneissl, M.; Seong, T.-Y.; Han, J.; Amano, H. The Emergence and Prospects of Deep-Ultraviolet Light-Emitting Diode Technologies. *Nat. Photonics* **2019**, *13*, 233−244.

(2) Li, D.; Liu, S.; Qian, Z.; Liu, Q.; Zhou, K.; Liu, D.; Sheng, S.; Sheng, B.; Liu, F.; Chen, Z.; et al. Deep-Ultraviolet Micro-LEDs Exhibiting High Output Power and High Modulation Bandwidth Simultaneously. *Adv. Mater.* **2022**, *34*, No. 2109765.

(3) Chen, J.; Loeb, S.; Kim, J.-H. LED Revolution: Fundamentals and Prospects for UV Disinfection Applications. *Environ. Sci.: Water Res. Technol.* **2017**, *3*, 188−202.

(4) Gerchman, Y.; Mamane, H.; Friedman, N.; Mandelboim, M. UV-LED Disinfection of Coronavirus: Wavelength Effect. *J. Photochem. Photobiol., B* **2020**, *212*, No. 112044.

(5) Amano, H.; Collazo, R.; Santi, C. D.; Einfeldt, S.; Funato, M.; Glaab, J.; Hagedorn, S.; Hirano, A.; Hirayama, H.; Ishii, R.; et al. The 2020 UV Emitter Roadmap. *J. Phys. D: Appl. Phys.* **2020**, *53*, No. 503001.

(6) Kuchuk, A. V.; Kryvyi, S.; Lytvyn, P. M.; Li, S.; Kladko, V. P.; Ware, M. E.; Mazur, Y. I.; Safryuk, N. V.; Stanchu, H. V.; Belyaev, A. E.; Salamo, G. J. The Peculiarities of Strain Relaxation in GaN/AlN Superlattices Grown on Vicinal GaN (0001) Substrate: Comparative XRD and AFM Study. *Nanoscale Res. Lett.* **2016**, *11*, No. 252.

(7) Akasaka, T.; Gotoh, H.; Kobayashi, Y.; Yamamoto, H. Extremely Narrow Violet Photoluminescence Line from Ultrathin InN Single Quantum Well on Step-Free GaN Surface. *Adv. Mater.* **2012**, *24*, 4296−4300.

(8) Kobayashi, H.; Ichikawa, S.; Funato, M.; Kawakami, Y. Self-Limiting Growth of Ultrathin GaN/AlN Quantum Wells for Highly Efficient Deep Ultraviolet Emitters. *Adv. Optical Mater.* **2019**, *7*, No. 1900860.

(9) Shan, M.; Zhang, Y.; Tian, M.; Lin, R.; Jiang, J.; Zheng, Z.; Zhao, Y.; Lu, Y.; Feng, Z.; Guo, W.; et al. Transverse Electric Lasing at a Record Short Wavelength 244.63 Nm from GaN Quantum Wells with Weak Exciton Localization. *ACS Photonics* **2021**, *8*, 1264−1270.

(10) Bayerl, D.; Kioupakis, E. Room-Temperature Stability of Excitons and Transverse-Electric Polarized Deep-Ultraviolet Luminescence in Atomically Thin GaN Quantum Wells. *Appl. Phys. Lett.* **2019**, *115*, No. 131101.

(11) Aiello, A.; Wu, Y.; Pandey, A.; Wang, P.; Lee, W.; Bayerl, D.; Sanders, N.; Deng, Z.; Gim, J.; Sun, K.; et al. Deep Ultraviolet Luminescence Due to Extreme Confinement in Monolayer GaN/Al(Ga)N Nanowire and Planar Heterostructures. *Nano Lett.* **2019**, *19*, 7852−7858.
(12) Toropov, A. A.; Evropeitsev, E. A.; Nestoklon, M. O.; Smirnov, D. S.; Shubina, T. V.; Kaibyshev, V. Kh.; Budkin, G. V.; Jmerik, V. N.; Nechaev, D. V.; Rouvimov, S.; et al. Strongly Confined Excitons in GaN/AlN Nanostructures with Atomically Thin GaN Layers for Efficient Light Emission in Deep-Ultraviolet. *Nano Lett.* **2020**, *20*, 158−165.
(13) Wu, F.; Zhang, J.; Wang, S.; Long, H.; Dai, J.; Feng, Z. C.; Gong, Z.; Chen, C. Quantum Confinement Dependence of Exciton Localization in A-Plane GaN/AlGaN Multiquantum Wells Investigated by Temperature Dependent Photoluminescence. *Opt. Mater. Express* **2015**, *5*, 2608−2615.
(14) Tasco, V.; Campa, A.; Tarantini, I.; Passaseo, A.; González-Posada, F.; Redondo-Cubero, A.; Lorenz, K.; Franco, N.; Muñoz, E. Investigation of Different Mechanisms of GaN Growth Induced on AlN and GaN Nucleation Layers. *J. Appl. Phys.* **2009**, *105*, No. 063510.
(15) Holec, D.; Zhang, Y.; Rao, D. V. S.; Kappers, M. J.; McAleese, C.; Humphreys, C. J. Equilibrium Critical Thickness for Misfit Dislocations in III-Nitrides. *J. Appl. Phys.* **2008**, *104*, No. 123514.
(16) Birner, S.; Zibold, T.; Andlauer, T.; Kubis, T.; Sabathil, M.; Trellakis, A.; Vogl, P. Nextnano: General Purpose 3-D Simulations. *IEEE Trans. Electron Devices* **2007**, *54*, 2137−2142.
(17) Moram, M. A.; Vickers, M. E. X-Ray Diffraction of III-Nitrides. *Rep. Prog. Phys.* **2009**, *72*, No. 036502.
(18) Muth, J. F.; Brown, J. D.; Johnson, M. A. L.; Yu, Z.; Kolbas, R. M.; Cook, J. W.; Schetzina, J. F. Absorption Coefficient and Refractive Index of GaN, AlN and AlGaN Alloys. *MRS Internet J. Nitride Semicond. Res.* **1999**, *4*, 502−507.
(19) Angerer, H.; Brunner, D.; Freudenberg, F.; Ambacher, O.; Stutzmann, M.; Höpler, R.; Metzger, T.; Born, E.; Dollinger, G.; Bergmaier, A.; et al. Determination of the Al Mole Fraction and the Band Gap Bowing of Epitaxial AlxGa1−xN Films. *Appl. Phys. Lett.* **1997**, *71*, 1504−1506.
(20) Kaganer, V. M.; Brandt, O.; Trampert, A.; Ploog, K. H. X-Ray Diffraction Peak Profiles from Threading Dislocations in GaN Epitaxial Films. *Phys. Rev. B* **2005**, *72*, No. 045423.
(21) Stanchu, H. V.; Kuchuk, A. V.; Barchuk, M.; Mazur, Y. I.; Kladko, V. P.; Wang, Z. M.; Rafaja, D.; Salamo, G. J. Asymmetrical Reciprocal Space Mapping Using X-Ray Diffraction: A Technique for Structural Characterization of GaN/AlN Superlattices. *CrystEngComm* **2017**, *19*, 2977−2982.
(22) Wallis, D. J.; Zhu, D.; Oehler, F.; Westwater, S. P.; Pujol, A.; Humphreys, C. J. Measuring the Composition of AlGaN Layers in GaN Based Structures Grown on 150 Mm Si Substrates Using (2 0 5) Reciprocal Space Maps. *Semicond. Sci. Technol.* **2013**, *28*, No. 094006.
(23) Tanner, B. K. Grazing Incidence X-Ray Reflectivity and Scattering. *Handbook of Advanced Nondestructive Evaluation*; Ida, N.; Meyendorf, N., Eds.; Springer International Publishing: Cham, 2019; pp 1181−1214.
(24) Vurgaftman, I.; Meyer, J. R. Band Parameters for Nitrogen-Containing Semiconductors. *J. Appl. Phys.* **2003**, *94*, 3675−3696.
(25) Tripathy, S.; Lin, V. K. X.; Dolmanan, S. B.; Tan, J. P. Y.; Kajen, R. S.; Bera, L. K.; Teo, S. L.; Kumar, M. K.; Arulkumaran, S.; Ng, G. I.; et al. AlGaN/GaN Two-Dimensional-Electron Gas Heterostructures on 200 Mm Diameter Si(111). *Appl. Phys. Lett.* **2012**, *101*, No. 082110.
(26) Tobaldi, D. M.; Triminì, V.; Cretì, A.; Lomascolo, M.; Dicorato, S.; Losurdo, M.; Passaseo, A.; Tasco, V. Low-Temperature and Ammonia-Free Epitaxy of the GaN/AlGaN/GaN Heterostructure. *ACS Appl. Electron. Mater.* **2021**, *3*, 5451−5458.
(27) Reshchikov, M. A.; Morkoç, H. Luminescence Properties of Defects in GaN. *J. Appl. Phys.* **2005**, *97*, No. 061301.
(28) Zhang, X. B.; Taliercio, T.; Kolliakos, S.; Lefebvre, P. Influence of Electron-Phonon Interaction on the Optical Properties of III Nitride Semiconductors. *J. Phys.: Condens. Matter* **2001**, *13*, 7053−7074.
(29) Nepal, N.; Li, J.; Nakarmi, M. L.; Lin, J. Y.; Jiang, H. X. Temperature and compositional dependence of the energy band gap of AlGaN alloys. *Appl. Phys. Lett.* **2005**, *87*, No. 242104.
(30) Ichikawa, S.; Funato, M.; Kawakami, Y. Dominant Nonradiative Recombination Paths and Their Activation Processes in Al x Ga 1 − x N -Related Materials. *Phys. Rev. Appl.* **2018**, *10*, No. 064027.
(31) Rigutti, L.; Mancini, L.; Lefebvre, W.; Houard, J.; Hernàndez-Maldonado, D.; Russo, E. D.; Giraud, E.; Butté, R.; Carlin, J.-F.; Grandjean, N.; et al. Statistical Nanoscale Study of Localised Radiative Transitions in GaN/AlGaN Quantum Wells and AlGaN Epitaxial Layers. *Semicond. Sci. Technol.* **2016**, *31*, No. 095009.
(32) Wang, Y.; Rong, X.; Ivanov, S.; Jmerik, V.; Chen, Z.; Wang, H.; Wang, T.; Wang, P.; Jin, P.; Chen, Y.; et al. Deep Ultraviolet Light Source from Ultrathin GaN/AlN MQW Structures with Output Power Over 2 Watt. *Adv. Opt. Mater.* **2019**, *7*, No. 1801763.
(33) Lähnemann, J.; Kaganer, V. M.; Sabelfeld, K. K.; Kireeva, A. E.; Jahn, U.; Chèze, C.; Calarco, R.; Brandt, O. Carrier Diffusion in $ \mathrm{Ga}\mathrm{N}$: A Cathodoluminescence Study. III. Nature of Nonradiative Recombination at Threading Dislocations. *Phys. Rev. Appl.* **2022**, *17*, No. 024019.
(34) Bigenwald, P.; Lefebvre, P.; Bretagnon, T.; GilBigenwald, B. Confined Excitons in GaN−AlGaN Quantum Wells. *Phys. Status Solidi B* **1999**, *216*, 371−374.
(35) Bayer l, D.; Islam, S. M.; Jones, C. M.; Protasenko, V.; Jena, D.; Kioupakis, E. Deep ultraviolet emission from ultra-thin GaN/AlN heterostructures. *Appl. Phys. Lett.* **2016**, *109*, No. 241102.
(36) Haughn, C. R.; Rupper, G.; Wunderer, T.; Yang, Z.; Johnson, N. M.; Wraback, M.; Garrett, G. A. Highly radiative nature of ultra-thin c-plane Al-rich AlGaN/AlN quantum wells for deep ultraviolet emitters. *Appl. Phys. Lett.* **2019**, *114*, No. 102101.
(37) Wu, Y.; Liu, X.; Wang, P.; Laleyan, D. A.; Sun, K.; Sun, Y.; Ahn, C.; Kira, M.; Kioupakis, E.; Mi, Z. Monolayer GaN excitonic deep ultraviolet light emitting diodes. *Appl. Phys. Lett.* **2020**, *116*, No. 013101.

https://doi.org/10.1021/acs.jpcc.2c04118
J. Phys. Chem. C 2022, 126, 14727−14734